

Searching for Signatures of Cosmic String Wakes in 21cm Redshift Surveys using Minkowski Functionals

Evan McDonough and Robert H. Brandenberger

Department of Physics, McGill University, Montréal, QC, H3A 2T8, Canada

(Dated: March 16, 2021)

Minkowski Functionals are a powerful tool for analyzing large scale structure, in particular if the distribution of matter is highly non-Gaussian, as it is in models in which cosmic strings contribute to structure formation. Here we apply Minkowski functionals to 21cm maps which arise if structure is seeded by a scaling distribution of cosmic strings embedded in background fluctuations, and then test for the statistical significance of the cosmic string signals using the Fisher combined probability test. We find that this method allows for detection of cosmic strings with $G\mu > 5 \times 10^{-8}$, which would be improvement over current limits by a factor of about 3.

I. INTRODUCTION

The interest in searching for the signatures of cosmic strings in cosmological observations has been increasing. This is due in part to the realization that cosmic strings can arise in a variety of cosmological contexts. For example, in many inflationary models (both supergravity-based [1] and string-based [2]) the period of inflation ends with the formation of a network of cosmic strings. Such strings may also be produced in conventional phase transitions which occur after inflationary reheating [55]. If they are topologically stable, the network of cosmic strings will persist at all times and will approach a ‘scaling solution’ characterized by a string distribution which is statistically independent of time if lengths are scaled to the Hubble radius (see e.g. [4–6] for reviews of cosmic strings and their consequences for cosmology).

Cosmic strings are linear topological defects which arise in a wide range of quantum field theories as a consequence of a symmetry breaking phase transition. They are lines of trapped energy density and tension which is equal in magnitude to the energy density. They are analogous to defect lines in crystals or to vortex lines in superconductors and superfluids, except for the fact that the cosmic strings arise in relativistic field theories and hence obey relativistic dynamical equations of motion as opposed to the strings in condensed matter systems whose dynamics is typically friction-dominated. The trapped energy density associated with the strings leads to consequences in cosmology which result in clear observational signatures. Since the energy density per unit string length increases as η^2 as the symmetry breaking scale η increases, cosmology provides the ideal venue to search for strings at very high energy scales. Thus, searching for strings in cosmological observations provides an avenue complementary to accelerator experiments for looking for signals of physics beyond the Standard Model: accelerator signals are more easily seen for low symmetry breaking scales, while signals in cosmology are more easily detected for larger values of η .

Because of the scaling solution of the cosmic string network, cosmic strings lead to a scale-invariant spectrum of cosmological perturbations, as in inflationary mod-

els (see e.g. [7]). However, the string-induced density fluctuations are highly non-Gaussian, an effect which is eliminated when computing the usual power spectrum of density fluctuations. It follows that string signals are much easier to detect in position space than in momentum space.

The scaling network contains two types of strings, a network of ‘infinite’ strings [56] and a distribution of string loops with radii smaller than the Hubble radius. String loops oscillate because of their relativistic tension and slowly decay by emitting gravitational radiation. Their gravitational effects are similar to those of a point mass [7]. In this paper we are interested in the characteristic non-Gaussian effects of long string segments and will not further consider cosmic string loops (which produce 21cm signals which are harder to differentiate from noise [8]).

Due to the relativistic tension of the strings, an infinite string segment will typically have a velocity in the plane perpendicular to the string which is of the order of the speed of light [57]. Since space perpendicular to a long straight string is conical with a ‘deficit angle’ given by [10]

$$\alpha = 8\pi G\mu, \quad (1)$$

where G is Newton’s constant and μ is the mass per unit length of the string (which is proportional to η^2), a string moving with velocity v_s through the matter gas of the early universe at some time t_i will lead to a ‘wake’ [11], a thin wedge behind the string with twice the background density whose planar dimensions are

$$c_1 t_i \times v_s \gamma_s t_i. \quad (2)$$

Here, γ_s is the relativistic γ factor associated with the velocity v_s , and c_1 is a constant of order one which is proportional to the curvature radius of the long string network in units of the Hubble radius. The mean thickness h of the wake is initially

$$h = 4\pi G\mu v_s \gamma_s t_i \quad (3)$$

and for $t > t_i$ it increases by gravitationally accreting matter from above and below the wake [12].

Current observations (in particular the oscillatory features in the angular power spectrum of cosmic microwave background (CMB) anisotropies) set an upper bound on the string tension of the order $G\mu < 1.7 \times 10^{-7}$ [13, 14], which corresponds to cosmic strings contributing less than 5% to the total spectrum of inhomogeneities. We will discuss this in more detail in section II. In this paper, we are therefore considering a setup in which there is a contribution of cosmic strings to the power spectrum in addition to the dominant component of Gaussian, nearly scale-invariant fluctuations (such as can be produced in inflationary cosmology [15, 16] or in string gas cosmology [3]).

Cosmic string wakes give rise to distinctive signatures in the large-scale distribution of matter in the universe. As discussed in [17], they lead to planar structures in the distribution of galaxies. Since wakes present between the time of last scattering of the CMB and today represent overdense regions of electrons, they lead to extra scattering of CMB photons and hence to distinctive rectangular regions in the sky with extra CMB polarization [18] (with statistically equal B-mode and E-mode components). The effect relevant to the current paper is that wakes represent overdense regions of neutral hydrogen and hence [19] lead to wedge-like regions in 21cm redshift surveys of extra 21cm absorption or emission [58]. The amplitude of the position space signal is independent of the string tension μ and can be as large as 100mK [59]. The width of the wedge, however, depends linearly on μ . A crucial point is that wakes exist as non-linear structures at high redshifts since as soon as the string passes by, a wake with overdensity 2 forms. This is to be contrasted to the situation in Gaussian models with a scale-invariant spectrum of primordial cosmological perturbations in which no nonlinear structures exist until quite low redshifts. In particular, at redshifts larger than that of reionization, the cosmic string signal should stand out against the effects of Gaussian fluctuations and noise. Thus, 21cm redshift surveys appear to be an ideal window to search for cosmic string signals.

If cosmic strings exist, then the induced 21cm maps will not only contain the characteristic wedges of extra absorption or emission. They will also contain noise, most importantly Gaussian noise from the primordial Gaussian density fluctuations which must be present in addition to the string-induced perturbations. Good statistical tools will be required in order to extract the string signals in a quantitative and reliable way.

In this report we study the possibility that Minkowski Functionals [21], a tool for characterizing structure which is orthogonal to the usual way of characterizing maps using correlation functions, can be applied to identify cosmic string signals in 21cm redshift surveys at redshifts larger than that of reionization. The theory behind Minkowski Functionals has its roots in Integral Geometry and Hadwiger's Theorem, which states that a d -dimensional set of convex bodies can be completely described by $d+1$ functionals. Minkowski functionals have

been applied numerous times in cosmology, e.g. to the distribution of galaxies on large scales [22] and the analysis of CMB maps [23]. There have also been attempts to apply Minkowski functionals to search for signatures of cosmic strings in the large-scale structure of the distribution of galaxies [24]. Since for 21cm redshift surveys the contributions to the 'noise' from the Gaussian source of primordial fluctuations is in the linear regime at the high redshifts we are interested in (larger than the redshift of reionization), we expect that Minkowski functionals will be very powerful in extracting cosmic string signals in the case of 21cm maps.

The outline of this paper is as follows: in the following section we outline current observational limits on cosmic strings as well as prospects for future detection. In Section III we briefly review the toy model for the cosmic string scaling distribution which we use and describe the theoretical 21cm maps induced by cosmic strings. Section IV then repeats the methodology of section III but including a simulation of the background noise. In Section V we review the theory and calculation of Minkowski functionals, before presenting our results in Section VI. We conclude with a summary of our results and a discussion of future work.

II. OBSERVATIONAL CONSTRAINTS

The strongest constraints on cosmic strings currently come from measurements of the angular power spectrum of the cosmic microwave background (CMB). The WMAP data provided no hints of cosmic strings, and hence placed an upper bound on the string tension [14]. Specifically, it constrained the string contribution to the primordial power spectrum to be less than 10%. However, there are now CMB experiments with better angular resolution than WMAP provided and which can yield improved bounds on the cosmic string tension. The Atacama Cosmology Telescope (ACT) [25], a six-meter off-axis telescope with arcminute-scale resolution located in the Atacama desert in northern Chile, and the South Pole Telescope (SPT) [26], a 10 meter telescope located in Antarctica which can study the small-scale angular power spectrum of the CMB, both are providing excellent data. A recent analysis of the angular power spectrum of CMB anisotropies from joint SPT and WMAP7 [13] made use of a Markov Chain Monte Carlo likelihood analysis to place a limit on the string tension of $G\mu < 1.7 \times 10^{-7}$ (at 95% confidence). This analysis was done in the context of the zero width cosmic string toy model which we will also use in the following. A similar limit was found by [27], who used combined WMAP7, QUAD and ACT data to place limits on the tension of Abelian Higgs model strings. The resulting bound on the string tension was $G\mu < 4.2 \times 10^{-7}$.

The difference in the results is mostly due to the uncertainties in the distribution of strings. Due to the very large range of scales involved (the width of a cosmic string

is microscopic but the length is cosmological), numerical simulations of both field theory and Nambu-Goto strings involve ad hoc assumptions and/or extrapolations. The uncertainties in the resulting string distributions appear in free parameters (e.g. the number of long string segments per Hubble volume and the value of the constant c_1) of toy models distributions of cosmic strings. These uncertainties effect the angular power spectrum of CMB anisotropies.

Local position space searches for signals of individual cosmic strings are less sensitive to the uncertainties in the string distribution than power spectra. This is the idea behind the proposal of [28–30] to search in position space for the line discontinuities in CMB anisotropy maps which long straight cosmic strings produce due to the Kaiser-Stebbins [31] effect. It was proposed to analyze position space anisotropy maps using of the Canny edge detection algorithm. It was shown [30] that strings with $G\mu \geq 10^{-8}$ might be detectable with this method. Application of this method to the SPT or ACT data may yield interesting results [60]

Another avenue for detection of cosmic strings is via gravitational waves, which will be produced by oscillating cosmic strings and/or the decay of cosmic string loops. Cosmic strings in fact [33] produce a scale-invariant spectrum of gravitational waves with an amplitude which is similar to or larger than the amplitude of gravitational waves from simple inflationary models. Pulsar timing [34] or direct detection (e.g. making use of the Laser Interferometer Gravitational-Wave Observatory (LIGO) [35]) provide means for searching for the cosmic string signal. However, at the moment the bounds are not competitive with bounds obtained from the CMB [61].

We are currently entering a revolution in radio astronomy, with both the Square Kilometer Array (SKA) [36] and the European Extremely Large Telescope (E-ELT)[37] aiming to be operational by early 2020. Of particular interest (in terms of potential to observe cosmic strings) is the SKA, which as the name implies will consist of 1 million square meters of collecting area. There are many ongoing projects to develop the science and technology necessary to operate the SKA. These are categorized into: (1) Precursor Facilities, which will physically be at the SKA site carrying out SKA-related projects, (2) Pathfinder Experiments, which will develop SKA-related science and technology off-site, and (3) Design Studies, which will investigate technologies and develop prototypes. Many of these projects are world class facilities in their own right, and we will mention some of the experiments which may have a chance of observing cosmic strings.

One such project is LOFAR [38], a Pathfinder experiment, which is measuring the neutral hydrogen fraction of the inter-galactic medium. This will map out the epoch of reionization between redshifts 11.5 and 6.7, and will be capable out of arc-minute resolution. For 21cm measurements, the redshift range of LOFAR extends to the “Dark Ages” before reionization, redshifts

where the cosmic string signal will be cleanest. Another SKA project with potential to observe cosmic strings is the MEERKAT experiment [39], which is carrying out a project titled MESMER that will track the neutral hydrogen content of the early universe by using carbon monoxide as a proxy. To make an accurate prediction as to the clumping of carbon monoxide around a cosmic string would require semi-analytical hydrodynamics calculations, but to a rough approximation we should expect to see the characteristic wedge of emission/absorption.

III. THE COSMIC STRING SIGNAL

A. Modelling the signal

In any theory which leads to the formation of stable cosmic strings in the early universe, a network of strings will persist at all later times, and this network will approach a ‘scaling solution’, meaning that the statistical properties of the network of cosmic strings are independent of time if all distances are scaled to the Hubble radius. The existence of the scaling solution can be argued for using analytical arguments (see e.g. [4–6]), and it has been confirmed using extensive numerical simulations [9].

The scaling distribution of strings consists of a network of long strings of mean curvature radius $\zeta = c_1 t$ (where c_1 is a constant of order 1), and string loops with a much smaller radius that result from intersection and hence ‘cutting’ of the long strings. As a consequence of their relativistic tension, the long strings have typical translational velocities v_s close to the speed of light. Hence, Hubble length string segments will intersect with other such segments with probability close to one on a Hubble time scale. By this process, string loops are formed and the correlation length of the long string network (the mean curvature radius) increases in comoving coordinates to keep up with the Hubble radius, as confirmed in the numerical string evolution simulations [9].

As is commonly done in studies of the cosmological consequences of cosmic strings, we use an analytical toy model of the infinite string network which was first introduced in [40]: we divide the time interval of interest (usually the time between the time t_{eq} of equal matter and radiation and the present time t_0) into Hubble time steps. In each time step we lay down an integer number N_H per Hubble volume of straight string segments of length $c_1 t$ with random midpoints and random tangent vectors. The string segments in neighboring Hubble time steps are taken to be independent. The long strings are taken to have a velocity v_s orthogonal to their tangent vectors. Each such string will produce a wake whose thickness grows in time.

We will be interested in signals which are emitted at a time $t_e > t_i$ from string wakes laid down at any time t_i between t_{eq} [62] and the present time. Since the planar dimensions of the wake (whose initial physical dimensions are given in (2)) are constant in comoving coordinates

dinates, their physical size grows with the scale factor. The comoving thickness of the wake, whose initial physical length is given by (3), grows linearly with the scale factor because of gravitational accretion. Hence, the dimensions of the wake at t_e in physical coordinates are given by:

$$\frac{z_i + 1}{z_e + 1} \left[c_1 t_i \times t_i v_s \gamma_s \times 4\pi G \mu t_i v_s \gamma_s \frac{z_i + 1}{z_e + 1} \right], \quad (4)$$

where z_e is the emission redshift $z(t_e)$.

The dominant form of the baryonic matter in the universe before reionization is neutral hydrogen (H), which we detect via the 21cm hyperfine line. Measuring the intensity of the redshifted 21cm radiation from the sky has the potential of giving us three dimensional maps of the distribution of neutral hydrogen in the universe (see e.g. [41] for an in-depth review article on 21cm cosmology). As explained in detail in [19], since wakes are overdense regions of neutral hydrogen, they will lead to excess 21cm emission or absorption. We will see this excess in directions for which our past light cone intersects a wake at some time $t_e > t_{rec}$, t_{rec} being the time of recombination. This 21cm signal has the special geometry given by the wake geometry - a thin wedge in the three-dimensional 21cm redshift survey (see Figure 1), and it is this special geometry which provides the ‘smoking gun’ signal for cosmic strings, the signal which we are trying to extract using Minkowski functionals in this report.

Since already at the initial time t_i the wake is a non-linear density fluctuation, the matter being accreted onto the wake will collapse onto the wake, shock heat and thermalize [63]. The hydrogen (H) atoms inside a wake laid down at redshift z_i will have a temperature at time t_e given by:[19]

$$T_K(t_e) = \frac{16\pi^2}{75} (G\mu)^2 (v_s \gamma_s)^2 \frac{z_i + 1}{z_e + 1} \frac{m}{k_B}, \quad (5)$$

where m is the proton mass. Inserting numerical values, and expressing $G\mu$ in units of 10^{-6} and so written as $(G\mu)_6$, we obtain

$$T_K(t_e) \approx [20K] (G\mu)_6^2 (v_s \gamma_s)^2 \frac{z_i + 1}{z_e + 1}. \quad (6)$$

Note that the numerical simulations by [43] show that the temperature can be taken to be approximately uniform inside of the wake.

The quantity of interest is the brightness temperature T_b due to 21cm transitions of the Hydrogen in the wake, or more specifically the difference δT_b in brightness temperature between photons from the wake and those from the surrounding space. From this point onwards, ‘brightness temperature’ will refer to δT_b , defined by

$$\delta T_b(z_e) = \frac{T_b(z_e) - T_\gamma(z_e)}{1 + z_e}, \quad (7)$$

where $T_\gamma(z_e)$ is the redshifted CMB temperature, and $T_b(z_e)$ is the brightness temperature due to 21 cm emission in the wake. A full derivation which can be found in [19] yields the following expression for δT_b :

$$\delta T_b(z_e) = [0.07K] \frac{x_c}{x_c + 1} \left(1 - \frac{T_\gamma}{T_K} \right) \sqrt{1 + z_e}, \quad (8)$$

where several constants have been absorbed into the prefactor, which can be found in the original derivation by [19]. Note that the collision coefficient x_c is given by [41]:

$$x_c = \frac{n \kappa_{10}^{HH} T_\star}{A_{10} T_\gamma}, \quad (9)$$

where T_\star , taken to be 0.068 K, is the temperature corresponding to the hydrogen energy splitting E_{10} , A_{10} is the spontaneous emission coefficient of the 21cm transition, n is the number density of hydrogen atoms, and κ_{10}^{HH} is the de-excitation cross section which is given in [41]. Using equation (8), the brightness temperature for a given wake with a given value of z_e can be obtained, which in conjunction with the spatial dimensions of the wake, allows a 3-D map of brightness temperature to be generated.

B. Generating Temperature Maps

In the following we will outline the steps in the construction of 21cm redshift maps in the case of primordial perturbations produced exclusively by strings. We will consider hypothetical sky maps covering a patch of the sky of angular scale $\theta \times \theta$. First, we must compute the number of strings which contribute to the sky signal in this patch. This is the number of strings whose wakes at some point in time between t_{rec} and t_0 intersect the observer’s past light cone with opening angle θ .

1. Distribution of Strings

According to our model of the distribution of a scaling string network we divide the time between t_{eq} and the present time t_0 into Hubble time steps. For each such time step centered at time t_i we now compute the number $N(t_i)$ of string wakes which at some point in the future of t_i will intersect the past light cone corresponding to an observational angle θ (a box of size $\theta \times \theta$ on the sky).

We first note that $N(t_i)$ is given by the ratio of the comoving volume of the past light cone

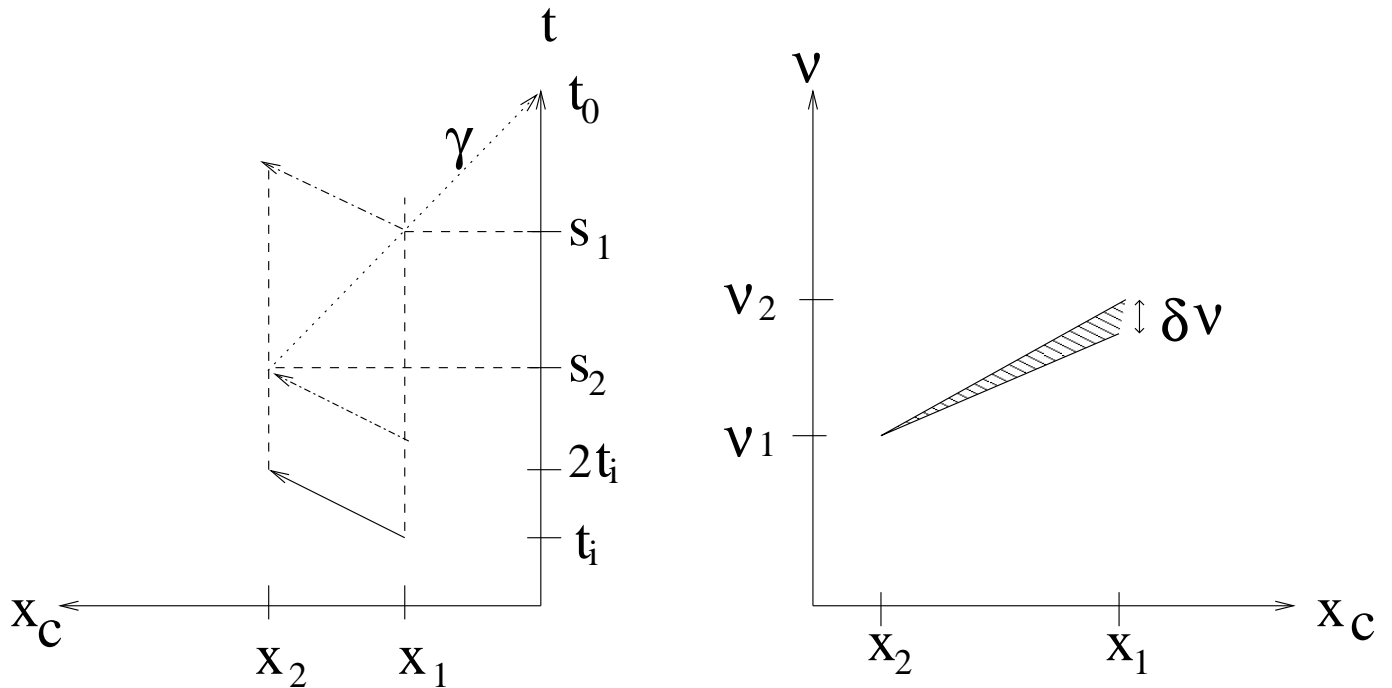
$$V_p(\theta) \simeq 27 \left(\frac{\theta}{2\pi} \right)^2 t_0^3 \quad (10)$$

divided by the comoving Hubble volume at time t_i

$$V_H(t_i) = t_i t_0^2, \quad (11)$$

multiplied by the number N_H of strings per Hubble volume in the scaling solution (a number which according

FIG. 1: The right panel depicts a sketch of the string wake-induced wedge of extra emission/absorption in 21cm redshift surveys. The horizontal axis represents the two angular directions, the vertical axis redshift. The left panel is a space-time sketch showing the position of the string which gives rise to the wedge of the right panel. Here, the vertical axis is time, and the horizontal axis corresponds to comoving spatial coordinates. Note, in particular, the positions where the string wedge intersects the past light cone of an observer at the current time t_0 . The almost horizontal lines represent the string at the time when it forms the wake (t_i), and the wedge at the times s_1 and s_2 when the back (and front) of the wake intersect our past light cone.



to numerical simulations is in the range $1 < N_H < 10$ [9]. This gives

$$N_i \simeq N_H 27 \left(\frac{\theta}{2\pi}\right)^2 z(t_i)^{3/2}. \quad (12)$$

Now that we know the total number of string wakes produced at redshift z_i which will be seen in the simulation box, we need to determine the distribution of the redshift z_e at which they will cross the past light cone of the simulation region in the sky. This can be determined by remembering that light travels in a straight line in conformal coordinates (comoving spatial coordinates and conformal time τ). Hence, the number of wakes which intersect the past light cone at conformal time τ (where the conformal time is measured backwards, meaning $\tau = 0$ at the present time and τ increases as we go back in time) in a conformal time interval $d\tau$ is

$$dN_i(\tau) = \left(\frac{\tau}{\tau_{eq}}\right)^2 \mathcal{N} d\tau, \quad (13)$$

where \mathcal{N} is determined by demanding that the integral over τ from $\tau_i \equiv \tau(t_i)$ to $\tau(t_0)$ gives N_i . The result can be integrated from 0 to τ_e to yield the number of string wakes $N_i(\tau_e)$ which intersect the past light cone at a time later or equal to τ_e :

$$N_i(\tau_e) = \left(\frac{\tau_e}{\tau_i}\right)^3 N_i. \quad (14)$$

To determine the redshift distribution of emission times z_e , we need to relate the conformal time τ_e to the emission redshift z_e . We start by expressing τ_e in terms of t_e ,

$$d\tau_e = \frac{dt_e}{a(t_e)}, \quad (15)$$

which evaluates to

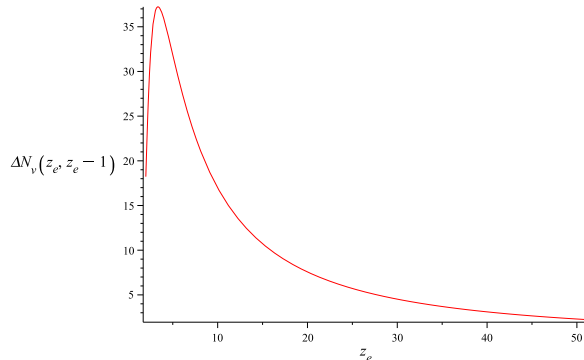
$$\tau_e = 3t_0 \left[1 - (z_e + 1)^{-\frac{1}{2}}\right]. \quad (16)$$

An expression for the number $N_i(z_e)$ of string wakes with an emission redshift larger or equal to z_e can now be obtained by substituting the preceding equation into equation 14, and using our expression for N_i from 12. This gives

$$N_i(z_e) = N_H 27 \left(\frac{\theta}{2\pi}\right)^2 z(t_i)^{3/2} \left[\frac{1 - (z_e + 1)^{-\frac{1}{2}}}{1 - (z_i + 1)^{-\frac{1}{2}}}\right]^3 \quad (17)$$

Due to the discrete nature of this simulation, we need to approximate this relationship by splitting the redshift space into slices, and laying down strings in each slice. The smallest possible slice would be the number of discrete values of redshift in the simulation (128, as we will discuss shortly) divided by the range of redshift, which we shall take to be 50 for this example. However, as we

FIG. 2: Distribution of the redshifts at which the string wakes intersect the past light cone (for a fixed time $z_i = 10^3$ at which the strings were produced). The horizontal axis is the emission redshift z_e , the vertical axis is the number $\Delta N_i(z_e, z_e - 1)$ of string wakes produced at redshift z_i (taken to be 10^3) which intersect the past light cone of the sky area we are considering in the redshift interval between $z_e - 1$ and z_e .



must have an integer numbers of wakes, a slice this small would result in the majority of slices having 0 wakes. Hence we instead choose a slice thickness $\Delta z_e = 1$, which will contain a number of wakes given by

$$\Delta N_i(z_e, z_e - 1) = [1.41 \times 10^6] \left[-2(x+1)^{-1/2} + 2x^{-1} - \frac{2}{3}x^{-3/2} \right]_{z_e-1}^{z_e}, \quad (18)$$

where we have included all prefactors into the constant. A plot of this distribution is shown in Figure 2. As is apparent, the largest number of wakes intersect the past light cone at low redshifts. This can be understood since the low redshift range covers most of the physical volume.

2. Angular and Redshift Scales of a Wake-Induced Wedge

As discussed in Section 2, each string wake which intersects the past light cone of the observer's angular patch will lead to a thin wedge of extra 21cm absorption or emission. We are concerned with string wakes produced at time t_i which intersect the past light cone of the observational patch at some time $t_e > t_{rec}$. Each such string wake will lead to a thin wedge in a 21cm redshift survey of a certain angular extent and certain thickness.

First, let us consider the angular extent of the wedge. A string laid down at a time t_i will create a wake with physical dimensions given by equation 4. To calculate the angular size of a wake, one must start with the physical length of the wake at time t_i which in direction tangent to the string is:

$$x_p(t_i) = c_1 t_i, \quad (19)$$

where (as we recall from before) c_1 is a constant of order 1. In the direction of string motion the size is the

same except that the factor c_1 gets replaced by $v_s \gamma_s$. In our work we choose the rather realistic parameter values where the two constants are the same. The corresponding comoving distance is then given by

$$x_c(t_i) = \left(\frac{t_0}{t_i} \right)^{\frac{2}{3}} x_p(t_i) = (z_i + 1)^{-1/2} c_1 t_0. \quad (20)$$

Hence, the corresponding angle θ_i is:

$$\theta_i = (z_i + 1)^{-1/2} c_1 \times 90^\circ. \quad (21)$$

For the most numerous and thickest wakes, $z_i + 1 = 1000$, and if the constant c_1 is taken to be $1/3$, the answer is then approximated by:

$$\theta_i = (z_i + 1)^{-1/2} \times 30^\circ \quad (22)$$

which yields approximately 1° as the angle of the wake-induced wedge.

Since the string which produces the wake is moving, the string-induced wake is slightly "tilted" in the three-dimensional redshift-angle space, i.e. the tip of the wedge (which corresponds to the string at the latest time) is at a slightly larger redshift than the mean redshift of the tail of the wedge (where the string was at the initial time). This does not change the fact that the projection of the wedge onto the angular plane has the dimension given above. However, when computing the projection into the redshift direction we have to be careful. The wedge is thin in direction perpendicular to the plane of the wedge, but this perpendicular direction is at an angle relative to the redshift direction. In the following we will compute the thickness of the wedge in perpendicular direction to the wedge plane.

We now calculate the thickness of the wake in the perpendicular direction. The finite thickness in redshift direction originates from the fact that photons originating from different parts of the wake are redshifted by slightly different amounts. The starting point of the computation is the formula

$$z + 1 = \left(\frac{t}{t_0} \right)^{\frac{2}{3}} \quad (23)$$

valid in the matter-dominated period. Taking differentials, and setting $t = t_e$ yields

$$\Delta z = \left(\frac{2}{3} \right) t_0^{-2/3} t_e^{-1/3} \Delta t_e, \quad (24)$$

where Δt_e is the time delay between photons from the top and the bottom of the wedge. We compute Δt_e at the midpoint of the wake (point of medium thickness). This is given by the thickness of the wake, which, as discussed in [19] grows linearly in comoving coordinates because of gravitational accretion onto the initial overdense region.

Using linear perturbation theory, the width of the wake at time t_e is

$$w(t_e) = 4\pi G \mu v_s \gamma_s t_0 (z(t_i) + 1)^{1/2} (z(t_e) + 1)^{-2}, \quad (25)$$

which equals Δt_e . Hence, from (24) it follows that

$$\Delta z = \frac{8\pi}{3} G_{\mu\nu s} \gamma_s (z(t_i) + 1)^{1/2} (z(t_2) + 1)^{-3/2}. \quad (26)$$

The analysis of gravitational accretion performed using the Zel'dovich approximation instead of with naive linear cosmological perturbation theory yields the same result [19] except that the coefficient is $24\pi/5$ instead of $8\pi/3$.

Once the dimensions of the wake are calculated, it remains to map this onto a 3-D lattice of points from which the Minkowski Functionals can be calculated. To do this requires setting the resolution with which the wakes will be studied, and then scaling up the dimensions of the wake. For the purposes of this simulator, we use a lattice of side length 128, and study a volume that subtends an angle of 10° in both the angular directions, with z_e ranging from 5 to 50, and $N_H = 3$. In this case, the angular resolution is $10^\circ/128 = .078^\circ$, while the resolution in the redshift direction is $45/128 = .35$. To scale up the dimensions of the wake only requires multiplying each dimension by the inverse of the resolution (ie: $128/45 = 2.84$ in the z_e direction).

3. Brightness Temperature: δT_b

The final step in the calculation is to determine the brightness temperature at every point of the three dimensional angle-redshift map (θ, ϕ, z) . Any point for which the past light ray in angular direction (θ, ϕ) does not intersect a wake at redshift z yields zero brightness temperature. A point which at redshift z_e is intersecting a wake due to a string present at time t_i is assigned a non-vanishing brightness temperature given by Equation (8), with T_K obtained from Equation (6). Overlapping wakes are assumed to be non-interacting.

IV. BACKGROUND NOISE

A. Modelling the Signal

As discussed in the introductory section, in our setup the cosmic strings only make a contribution of less than 5% to the total power spectrum of inhomogeneities. The dominant contribution is in the form of an approximately scale-invariant spectrum of Gaussian perturbations such as can be produced in a number of cosmological scenarios, e.g. in inflationary cosmology [16] or in string gas cosmology [3]. The dominant Gaussian fluctuations are in the linear regime until late times on large length scales and are hence not expected to contribute a lot to 21cm fluctuations at high redshifts (redshifts before reionization). There will, however, be smaller scale fluctuations which become non-linear, forming so-called ‘‘mini-halos’’ which then contribute to the spectrum of 21cm fluctuations. It is crucial for us to check that the cosmic string

effects can be detected above the noise from the Gaussian fluctuations (which we call ‘‘background noise’’ in the following).

The contribution of ‘‘background noise’’ to the 21cm fluctuations of the universe has been studied in detail (see e.g. [44, 45]). As was shown, there is an effect on 21cm maps which comes from the diffuse inter-galactic medium (IGM). However, this effect is homogeneous in space on the cosmological scales which interest us here and will hence not be further considered in this paper. Instead, we focus on the contribution of the inhomogeneities mentioned above which lead to the formation of mini-halos. This contribution has been studied done both semi-analytically, [44], and later using large scale numerical simulations [45].

To calculate the signal from minihalos we must find the mass function dn/dM , which can, when integrated over a range of masses, give the number density for minihalos in this mass range. There are two possible mass profiles for minihalos, the Sheth-Tormen model and the Press-Schechter model. Recent numerical simulations support the Press-Schechter model, (see Figure 2 of [45]). Once we know the mass function, the brightness temperature is then calculated using line of sight integrals given a realization of the inhomogeneities described by the mass function.

The Press-Schechter function for the number density of minihalos is given by [46]:

$$N(M)dM = - \left(\frac{\bar{\rho}}{M}\right) \left(\frac{2}{\pi}\right)^{1/2} \frac{\delta_c}{\sigma^2} \frac{d\sigma}{dM} e^{-\frac{\delta_c^2}{2\sigma^2}} dM \quad (27)$$

where $\bar{\rho}$ is the mean (baryonic and dark) matter density of the universe, and $\sigma^2(M, t) = \langle \delta_M^2 \rangle(t)$ is the root mean square mass fluctuation on the mass scale M . Halos will form in regions with a δ_M above a critical fluctuation $\delta_c \approx 1.69$. Our number density simplifies to:

$$\begin{aligned} N(M, z)dM &= \Omega_m \left(\frac{3+n}{6}\right) \left(\frac{\bar{\rho}}{M^2}\right) \\ &\times \left(\frac{2}{\pi}\right)^{1/2} \left(\frac{M}{M_*(z)}\right)^{\frac{(3+n)}{6}} \\ &\times \exp\left[-\frac{1}{2} \left(\frac{M}{M_*(z)}\right)^{(3+n)/3}\right] dM \end{aligned} \quad (28)$$

where M_* is the mass scale for which the fractional density fluctuation equals δ_c , and where we assume a primordial power spectrum of density fluctuations $P(k) \approx k^n$ (here, $P(k)$ does not contain the phase space factor k^3 and is not dimensionless. A scale-invariant spectrum of curvature fluctuations corresponds to $n = 1$).

The spatially averaged brightness temperature of a set of halos is given by [44]:

$$\delta \bar{T}_b = \frac{c(1+z)^4}{\nu_0 H(z')} \int_{M_{min}}^{M_{max}} \Delta \nu_{eff} \delta T_{b, \nu_0} A \frac{dN}{dM} dM \quad (29)$$

where $\Delta\nu_{eff}$ is the redshifted effective line width, $\delta T_{b,\nu_0}$ is the brightness temperature of individual minihalo at the frequency ν_0 , and A is the geometric cross section of the minihalo. The integral (worked out in [47] - see Figure 3 in that paper) yields a noise temperature which peaks at a value of 4mK at a redshift of 10 and decays at higher redshifts.

B. Generating Noise Temperature Maps

Given that the signal from the IGM is spatially uniform, we focus on the contribution from minihalos. The corresponding noise temperature maps are constructed by modeling the spatial fluctuations as a three-dimensional Gaussian random field with a power spectrum $P_T(k)$ (again defined without the phase space factor k^3) with a slope which will be discussed below, and with a variance given by (29). The amplitude of the resulting noise is rescaled in redshift direction by incorporating the redshift dependence of the variance from (29).

To accomplish this, we follow the procedure laid out in [30], which we generalize to 3 spatial dimensions, We can expand the spatial fluctuations in temperature into hyperspherical harmonics.:

$$\frac{\Delta T}{T}(\theta, \phi, \psi) = \sum_{l,m,n} a_{l,m,n} Y_{l,m,n}(\theta, \phi, \psi), \quad (30)$$

where the $Y_{l,m,n}$ are the spherical harmonics generalized to 3+1 dimensions, the ‘*hyperspherical harmonics*’, and the $a_{l,m,n}$ are the coefficients of this expansion. We can simplify this expression to a sum of plane waves, by making the flat sky approximation (valid for angular scales $< 60^\circ$). This gives us:

$$\tilde{T}(\vec{x}) = \sum_{\vec{k}} \tilde{T}(\vec{k}) e^{i\vec{k}\cdot\vec{x}} \quad (31)$$

where we have used the abbreviation $\tilde{T}(\vec{x}) \equiv \frac{\Delta T}{T}(\vec{x})$. Comparing this decomposition with our previous expression in terms of hyperspherical harmonics, we see that the $\tilde{T}(\vec{k})$ correspond to the $a_{l,m,n}$ and hence the $\tilde{T}(\vec{k})$ give us the power spectrum:

$$\langle \tilde{T}(\vec{k})^2 \rangle = \langle a_{l,m,n}^2 \rangle \sim P_T(k) \quad (32)$$

where the temperature power spectrum P_T is defined by the last equality.

Since the mini-halos are produced by the density fluctuations we use the power spectrum of density fluctuations to determine the slope of $P_T(k)$. Thus, we take $P_T(k)$ to be proportional to the primordial power spectrum:

$$P_T(k) \propto k^n \text{ with } n = 1. \quad (33)$$

and the amplitude is determined by demanding that the variance is given by (29). First, in fact, we generate

a three-dimensional Gaussian random field T_{GRF} with variance 1.

Note that in a model with a primordial scale-invariant spectrum of curvature perturbations, the dimensionless power spectrum of fractional density perturbations is approximately scale-invariant on scales which entered the Hubble radius before the time of equal matter and radiation. This is a consequence of the processing of the primordial spectrum which happens on sub-Hubble scales (see e.g. any text which discusses the Newtonian theory of cosmological perturbations, e.g. [48]). The spectrum on small scales thus takes on a slope $n = -3$. We do not consider this effect in the current simulations.

Using the ergodic hypothesis, we construct a Gaussian noise field by drawing the $\tilde{T}(\vec{k})$ for fixed $k = |\vec{k}|$ from a Gaussian distribution with power given by $P_T(k)$ and amplitude chosen to give variance 1.

We do our calculations on a lattice of $(\tilde{k}_1, \tilde{k}_2, \tilde{k}_3)$ coordinate values ranging from 0 to $N_{max} - 1$. We convert to the corresponding k values with:

$$k_i = \frac{2\pi}{L}(\tilde{k}_i - k_{max}) \quad (34)$$

where k_{max} corresponds to the angular resolution of the lattice in the k_i direction.

We can then calculate the $\tilde{T}(\vec{k})$ using:

$$\tilde{T}(\vec{k}) = \sqrt{\frac{P_T(k)}{2}} (g_1(\vec{k}) + ig_2(\vec{k})) \quad (35)$$

where g_1 and g_2 are randomly generated from a Gaussian distribution with variance 1 and mean 0, and we enforce $\tilde{T}(\vec{k}) = \tilde{T}(-\vec{k})$ to ensure that $T(\vec{x})$ is real.

We can then construct a spatial map by taking the inverse Fourier transform of the preceding expression. The result of this is a Gaussian random field T_{GRF} with a correlation function specified by the power spectrum and variance 1. We now wish to enforce the redshift dependence of the amplitude, which we do by identifying redshift z with the third spatial direction. Hence the final noise field is specified by:

$$T_{noise}(x, y, z) = \delta\bar{T}_b(z) T_{GRF}(x, y, z) \quad (36)$$

with amplitude $\delta\bar{T}_b(z)$ given by (29). Note that since the change in amplitude is uniform over the angular directions, this introduces deviations from strict Gaussianity of the the three-dimensional distribution.

V. INTEGRAL GEOMETRY AND MINKOWSKI FUNCTIONALS

Minkowski Functionals are a useful tool to analyze the topology of a d -dimensional map. Originally, these functionals were considered in the context of describing the topology of a body B embedded in a d -dimensional Euclidean space using an approximation in which the body

B was approximated by the set of convex bodies of a particular form but varying size (hence we have functionals and not just functions). In our application we will consider the Minkowski functionals as functionals of the class of bodies (termed an ‘excursion set’) which enclose regions of the map where the value of the variable which is mapped is larger than a cutoff value and we consider varying the cutoff value. For example, applied to CMB temperature anisotropy maps we consider bodies which are regions of the sky where the temperature T is larger than a cutoff temperature T_c whose amplitude we vary. In the case of interest here we consider three dimensional 21cm brightness temperature maps and we consider the topology of the volumes which contain points where the temperature exceeds a critical temperature whose magnitude we vary.

Minkowski first developed these functionals [49] in 1903 to solve problems of stochastic geometry [50]. This then led to the development of Integral Geometry in the mid 1900’s. At the heart of Integral Geometry is Hadwiger’s Theorem [21], which deals with the problem of characterizing the topology of the body B using scalar functionals V . These functionals must satisfy certain requirements [51]:

1. **Motion Invariance** : The functionals should be independent of the position and orientation in space of the body.
2. **Additivity**: The functionals applied to the union of two bodies equal the sum of their functionals minus the functionals of their intersection:

$$V(A \cup B) = V(A) + V(B) - V(A \cap B). \quad (37)$$

3. **Conditional Continuity**: The functionals of convex approximations to a convex body converge to the functionals of the body.

Hadwiger’s Theorem [21] states that for any d dimensional convex body, there exist $d+1$ functionals that satisfy these requirements, denoted $V_j, j = 0, \dots, d$, for the j ’th functional. Furthermore, these functionals provide a *complete* description of topology of the body. Mathematically, the j ’th functional of a d -dimensional body B is an integral over a $(d-j)$ -dimensional surface of B . For example, in three dimensions, the first functional V_0 is simply the volume of the body, and the second (V_1) is the surface area. In all dimensions, the last functional V_j is given by the Euler characteristic χ , which in three dimensions is defined [51] as:

$$\chi = \text{number of components} - \text{number of tunnels} \\ + \text{number of cavities}. \quad (38)$$

The simplest example is a set of balls of radius r_i . When r_i is very small, there are no intersections of balls, and χ is very close to the number of balls. As r_i increases, the balls will begin to intersect, creating tunnels. Thus

TABLE I: Geometric Interpretation of Minkowski Functionals in 1,2, and 3 dimensions [50]

d	1	2	3
V_0	length	area	volume
V_1	χ	circumference	surface area
V_2	-	χ	total mean curvature
V_3	-	-	χ

χ will become negative. At a certain threshold value of r_i , χ will once again be positive, as tunnels are cut off to form cavities. Finally, when r_i becomes very large, the entire space is filled, and χ is equal to 0.

The geometric meaning of the functionals for $d \leq 3$ is summarized in Table I [50]. A key feature of Minkowski Functionals is that they incorporate information about correlation functions of arbitrary order [50]. Hence, the Minkowski Functionals are much more sensitive to non-Gaussianity than a three or four point correlation function, making them an ideal tool to search for signatures of topological defects such as cosmic strings. An important fact is that exact expressions exist for a Gaussian Field (given by Tomita in [52]), allowing for a visual comparison between string-based and Gaussian maps (since all we have to look for is statistically significant deviations from the curves for a Gaussian distribution). We will apply this method in Section 6.

Next we will apply Minkowski functionals to the temperature maps whose construction is described in the previous section. For any fixed value of the temperature, we consider the corresponding iso-temperature surface. The Minkowski functionals probe the topology of this set of surfaces (or equivalently the bodies they enclose). They are calculated as a function of the temperature threshold, and the results are plotted as a function of this threshold. It is standard practice to use as the x axis not the actual value of the field, but a variable $\nu = f(x)/\sigma$ which is the number of standard deviations σ by which the value of the field $f(x)$ (scaled to have zero spatial average) deviates from zero. Hence, a rescaled threshold $\nu = \pm 1$ implies a fluctuation of the field by one standard deviation from the average value. The reason for using ν is to remove the effect of a constant factor on the functionals, and hence to allow for a comparison with structure that may be identical in every way but the magnitude of the temperature. For the purposes of this simulator, we calculated the functionals for the range $-4 \leq \nu \leq 4$.

The calculation of the Minkowski functionals was done using the program *Minkowski3*, written by Thomas Buchert. This piece of software takes a 3-D array of floats as input (in binary format), and outputs two estimates (with error values) of the Minkowski Functionals as well as the functionals for a Gaussian field. The two estimates for the Minkowski functionals correspond to two methods, one derived from differential geometry and the other from integral geometry. As a full derivation of each can

be found in [53], only a brief explanation will be provided here.

In the context of differential geometry, it is possible to describe all local curvature in terms of geometric invariants (Koenderink Invariants). We then express the global Minkowski functionals V_k in terms of the local Minkowski functionals $V_k^{(loc)}$, which are calculated in [53]. For the three dimensional case, the functionals of a field $\nu(\mathbf{x})$ in a volume \mathcal{D} are given by

$$V_k(\nu) = \frac{1}{|\mathcal{D}|} \int_{\mathcal{D}} d^3x \delta(\nu - \nu(\mathbf{x})) |\nabla \nu(\mathbf{x})| V_k^{(loc)}(\nu, \mathbf{x}). \quad (39)$$

In the discrete case, this is equivalent to summing over the lattice and taking a spatial average.

In the context of integral geometry, the Minkowski Functionals are calculated using Crofton's Formula. This provides a very elegant expression for the k 'th functional of a d dimensional object K , in a volume that consists of L lattice points of cubic lattice spacing a :

$$V_k^{(d)}(K) = \frac{\omega_d}{\omega_{d-k} \omega_k} \frac{1}{a^k L} \sum_{j=0}^k (-1)^j \frac{k!(d-k+j)!}{d!j!} N_{d-k+j}(K), \quad (40)$$

where ω_j is the volume of a j -dimensional unit sphere, and $N_j(K)$ is the number of j -dimensional lattice cells contained in K . For example, $N_0(K)$ is the number of lattice points in K , and $N_3(K)$ gives the number of cubes contained within K .

VI. RESULTS

A. Functionals of Cosmic Strings

We first consider the Minkowski Functionals of the wake signal alone, by taking a scaling solution of strings with $(G\mu)_6 = 0.17$, using the notation $(G\mu)_6 = G\mu \times 10^{-6}$. The results are shown in Figure 3. The four boxes show the mean Minkowski functionals after 100 simulations, with the errors taken to be the standard deviation. In each box, the green curve is based on calculating the functionals using the method of Koenderink Invariants, and the red curve is based on using the Crofton Formula (the red and green curves are almost perfect replicas of one another, and so the green is only visible in regions where they differ).

Since the number density of wakes is peaked around high redshift, the mean brightness temperature fluctuation δT_b will be negative, and hence the threshold value $\nu = 0$ corresponds to a slightly negative brightness temperature fluctuation. The threshold value ν_c corresponding to $\delta T_b = 0$ is a small positive number. It is at this threshold value that the four Minkowski functionals change abruptly. For $\nu > \nu_c$ the volume with δT_b greater than the threshold value vanishes, and hence the functionals V_1, V_2 and V_3 vanish. For $\nu < \nu_c$ the high temperature volume does not vanish, but it corresponds

to the outside of the wakes as opposed to the inside. Hence, the integrated mean curvature is negative. The key feature to notice in these plots is the abrupt change that occurs at the threshold value and the asymmetry about this threshold.

B. Functionals of Noise

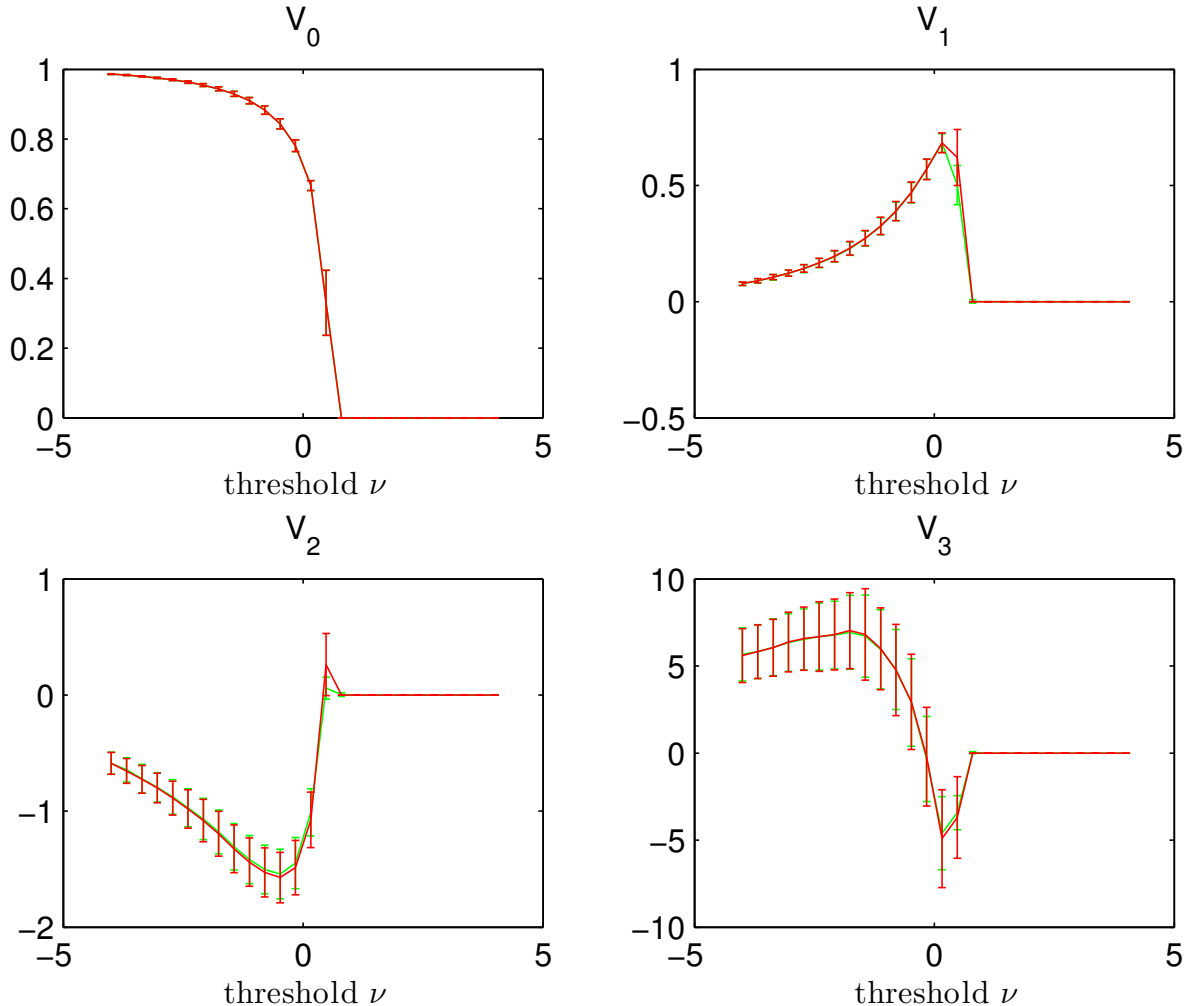
We now turn our attention to the Minkowski Functionals of the background noise due to minihalos, shown in Figure 4, where we again calculate the average functionals over 100 simulations and indicate the standard deviation with error bars. The corresponding functionals for a Gaussian random field are shown as the dashed black curves, whereas the functionals for the noise maps are shown in red and green. The key feature of these plots is the symmetry (or antisymmetry in the case of V_2 and V_0) about 0, which matches the results for a Gaussian random field. However the noise map functionals all share the common characteristic of being tightly concentrated about 0, which allows the noise map to be differentiated from a pure Gaussian random field. As mentioned above, the deviation of the noise maps from being a pure Gaussian random field comes from the scaling of the amplitude with redshift which is uniform over the two angular coordinates.

C. Functionals of Cosmic Strings Embedded in Noise

Armed with our knowledge of the behaviour of the Minkowski Functionals for both pure cosmic string wake and background noise maps, we can start with the real fun: differentiating maps of wakes and noise from maps of pure noise. To do this, we generate a map of wakes and noise by adding (at every point in space) the temperature fluctuations from wakes and the fluctuations from the mini-halo noise maps. We can then compare the Minkowski functionals as we vary the string tension, allowing us to place constraints on the minimum string tension necessary for the strings to be detected via this method.

For each value of the string tension $G\mu$ we performed 100 simulations. For each simulation we computed the χ^2 significance value of the difference between the string and a pure noise map. This was done in the following way: For each threshold bin i (we used $N_{bins} = 25$ threshold bins per functional, and hence $4 \cdot N_{bins} = 100$ bins in total) we computed the probability p_i that the Minkowski functional values for the string simulation come from the same distribution as obtained from the pure noise maps. We then combined the results of different bins into a χ^2

FIG. 3: Minkowski functionals of a pure scaling solution of cosmic string wakes, with $G\mu = 0.17 \times 10^{-6}$. Each of the four boxes shows the results for one of the four functionals, averaged over 100 simulations each using a lattice of 128^3 pixels. Each box contains two curves, corresponding to computing the functionals computed making use of one of the two methods, either Koenderink Invariants (the green curve) or the Crofton Formula (the red curve).



value using the Fisher combined probability test

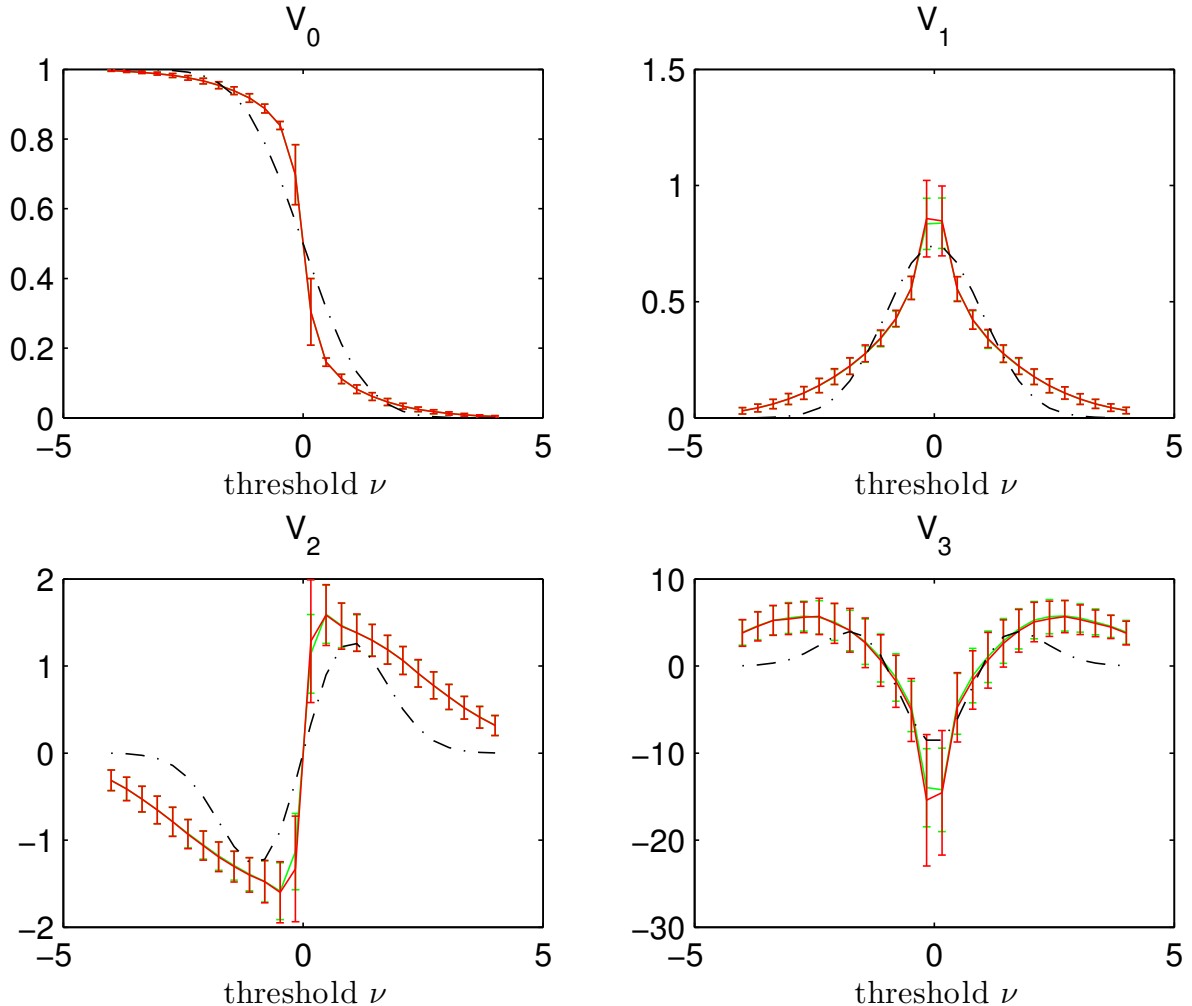
$$\chi^2 = -2 \sum_{i=1}^{4N_{bins}} \log(p_i). \quad (41)$$

We then computed the mean value $\bar{\chi}^2$ and the standard deviation $\Delta\chi^2$ of χ^2 . The criterion for significance of the difference between string wake and noise maps is that the value of $\bar{\chi}^2 - \Delta\chi^2$ is larger than the representative significance value for an analysis with $2(4N_{bins}) = 200$ degrees of freedom.

A comparison of the functionals of (wakes+noise) against pure noise is shown in Figures 5 to 8, which were done using a lattice size of 128^3 , each for a different value of $G\mu$. In each set of graphs, the black curves represent the results for the pure noise maps (the mean values and

standard deviations for each threshold value are shown), and the orange curves (the less symmetric - in the case of V_1 and V_3 - or less antisymmetric - in the case of V_0 and V_2 curves) represent what is obtained for maps containing both strings and noise. What is shown are the Minkowski functionals for a particular cosmic string wake simulation. The mean value of χ^2 was found to be greater than 10^3 (the maximal value our numerics could handle) for $G\mu \geq 6.7 \times 10^{-8}$, showing that for these values of $G\mu$ string maps can indeed be distinguished from pure noise maps. For $G\mu = 4.2 \times 10^{-8}$ the χ^2 drops down to 223 ± 101 , which indicates a good chance that any one set of wakes+noise will be indistinguishable from the noise at this value of $G\mu$. Hence from this preliminary analysis we conclude that the minimum string tension $G\mu$ must be roughly 5×10^{-8} for the Minkowski functional method

FIG. 4: Minkowski functionals of the background noise, averaged over 100 simulations each using a lattice of 128^3 pixels. Each box contains three curves. Two of them are for the noise map with the functionals computed making use of one of two estimates, either Koenderink Invariants (the green curve) or the Crofton Formula (the red curve). The dashed black curves give the Minkowski functionals for a Gaussian map.



to be able to detect the cosmic string signals which are embedded in the noise.

Note the V_i values for the cosmic string simulations in Figure 5 vanish to the level of the numerical accuracy above a certain value of the threshold, while those for noise alone do not. The reason this happens is that in the presence of string wakes, a fixed threshold value corresponds to a different brightness temperature than it would in the absence of strings.

Given the limited accuracy of the analysis, we know that the Minkowski functionals at sufficiently close threshold values are not independent. We must thus consider the possibility that we might have oversampled and

obtained an artificially large value of χ^2 . Put another way, since the temperature resolution δT of our maps is non-zero, we must account for this in our choice for the threshold bin resolution $\delta\nu$. We can relate $\delta\nu$ and δT by

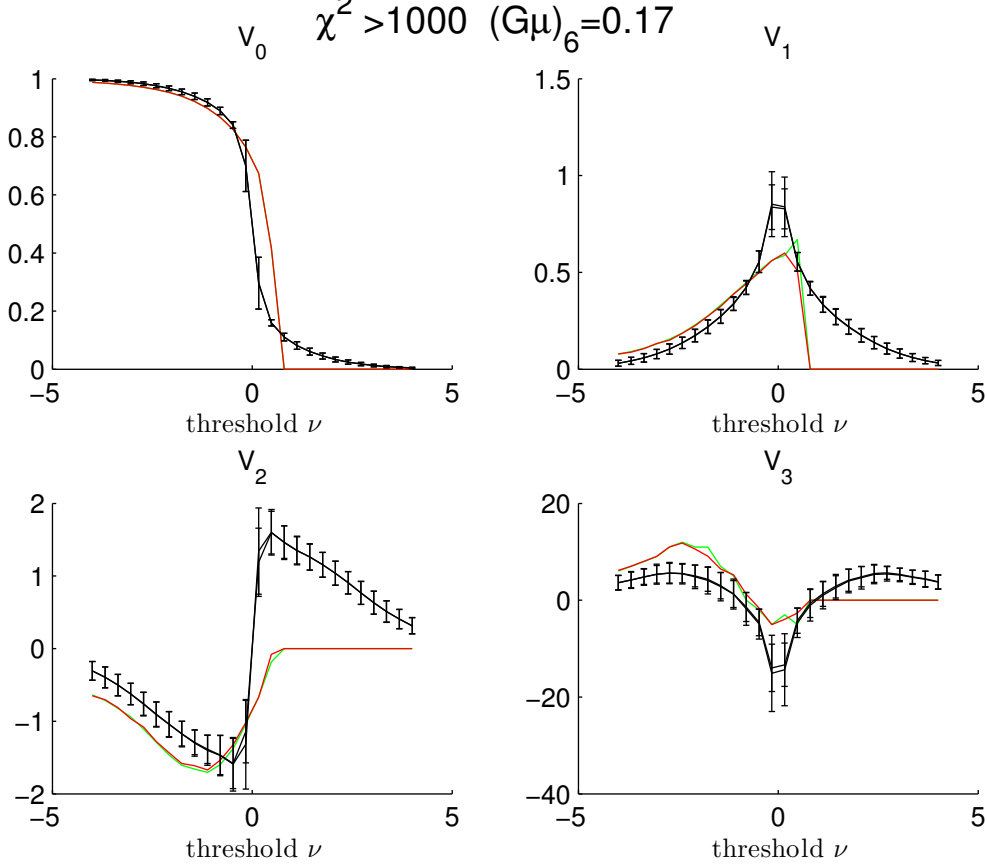
$$\delta\nu = \frac{\delta T}{\sigma_T}. \quad (42)$$

The temperature resolution can be estimated to first order by

$$\delta T = \delta x \cdot \nabla T, \quad (43)$$

where δx is the spatial resolution and ∇T is the gradient of the background noise. Since the resolution of the maps is the worst in the redshift direction, we focus on resolution in the z -direction. The relevant quantity then

FIG. 5: Minkowski functionals of a combined map (wakes+noise) with $G\mu = 1.7 \times 10^{-7}$ along with the corresponding functionals for a pure noise map, averaged over 100 simulations each using a lattice of 128^3 pixels. The black curves are for the pure noise maps, the orange ones for the strings+noise maps.



is the spatial resolution δl corresponding to the redshift resolution δz , which is given by

$$\delta l(\delta z, z) \sim c(\delta z)t_0 z^{-3/2}. \quad (44)$$

To then calculate the gradient ∇T , we use the fact that that the matter power spectrum is dominated by modes around $k \sim 1/\lambda_{eq}$, and hence this sets the length scale of the problem. We can then estimate the gradient by

$$T = \frac{\bar{T}}{\lambda_{eq}}, \quad (45)$$

where λ_{eq} is

$$\lambda_{eq} \sim ct_{eq}z_{eq}^{-1/2}. \quad (46)$$

Putting this all together we find

$$\delta T \sim \bar{T} \left(\frac{\delta z}{z} \right) \left(\frac{z_{eq}}{z} \right)^{1/2} \sim 0.05 \text{mK}, \quad (47)$$

where for the second equality we take $z = 50$. Using equation 42, this corresponds to $\delta\nu = 0.036$. We can

then translate that into an upper bound on the number of threshold bins we should use to span 8 standard deviations (-4σ to 4σ) and find

$$N_{bins} = \frac{8}{\delta\nu} \sim 200. \quad (48)$$

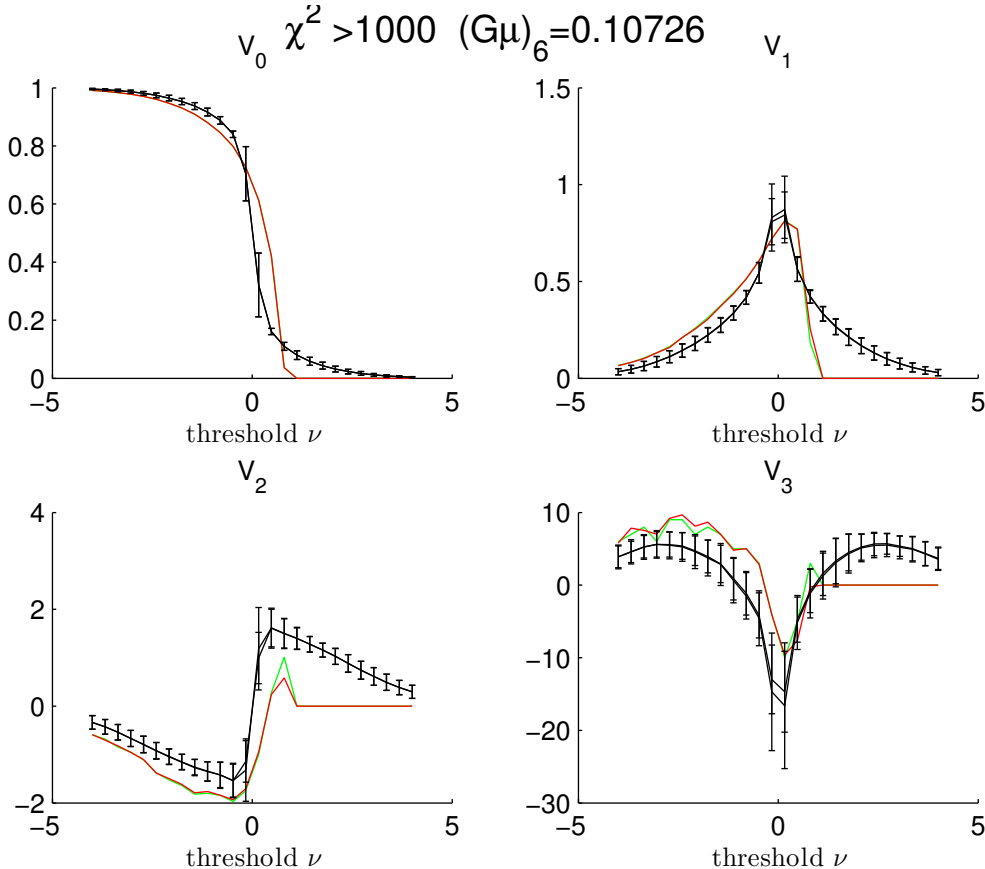
Hence our choice of 25 threshold bins is well within the limit from oversampling.

Another way to see that the bins can be treated as independent is to consider the correlation matrix for each functional. The correlation matrix is defined by

$$Corr_{ij} = \frac{Cov_{ij}}{\sigma_i \sigma_j} = \frac{\langle (X_i - \mu_i)(X_j - \mu_j) \rangle}{\sigma_i \sigma_j} \quad (49)$$

where the X_i are defined by the wake+noise signal for the i 'th bin. Hence i runs from 1 to 25, each X_i is a random variable that we have sampled 100 times (once for each trial of the simulation), and $\langle \rangle$ denotes expectation value. From each X_i we define a mean $\langle X_i \rangle = \mu_i$ and a standard deviation σ_i . From this we can calculate the correlation in the wake signal between the bins for each functional, as is plotted in Figure 9. For each functional, the correlation matrix is concentrated in a narrow

FIG. 6: Minkowski functionals of a combined map (wakes+noise) with $G\mu = 1.07 \times 10^{-7}$ along with the corresponding functionals for a pure noise map, averaged over 100 simulations each using a lattice of 128^3 pixels.



strip along the diagonal with a width at half max of 2-3 bins. Given this diagonal structure, we are safe from any hidden correlation that would invalidate our use of the Fisher combined probability test.

VII. SUMMARY AND OUTLOOK

This purpose of this investigation has been to both demonstrate the power of Minkowski Functionals for detecting non-Gaussian behaviour, and to investigate the topology of 21cm distributions in cosmological models with a scaling distribution of cosmic string wakes. We generated 3-D maps of the 21cm brightness temperature in pure cosmic string models, in models with only background noise from mini-halos, and in maps in which both sources of 21cm fluctuations were present, using methods similar to those employed for constructing 2-D CMB temperature by [30]. These maps were then be investigated with Minkowski functionals, using the software ‘*Minkowski3*’ made available by Buchert [54]. For large values of the string tension, the non-Gaussian signatures of string wakes are clearly visible in the Minkowski functionals. We studied for which range of values of the string

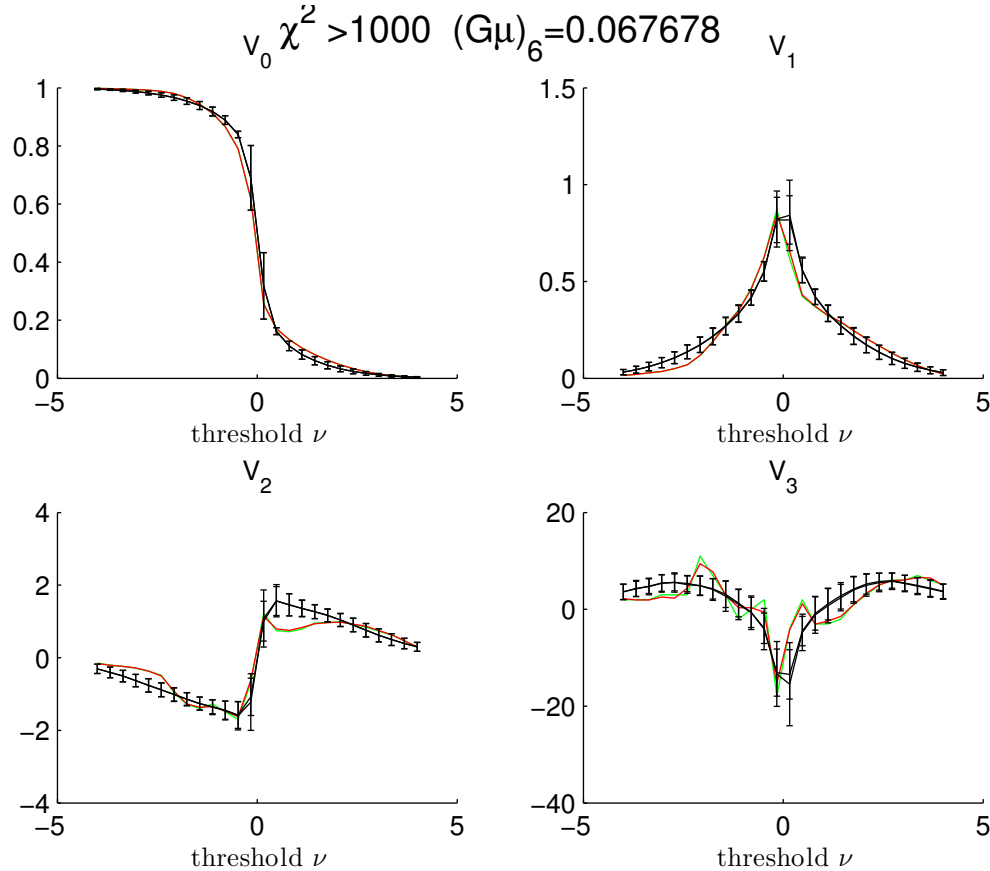
tension the difference between the strings + noise versus the pure noise maps as seen in the Minkowski functionals are statistically significant. A large difference was found between the functionals of the string-induced brightness temperature map and the corresponding functionals of background noise, with maps of strings embedded in noise found to be differentiable from maps of pure noise when $G\mu > 5 \times 10^{-8}$.

The analysis presented in this report serves as a proof of concept that the Minkowski functionals can be used as a statistical tool to search for cosmic string signals. To extend this preliminary analysis would mean performing large scale numerical simulations, as new features may present themselves as we study the 21cm maps with greater resolution.

Acknowledgments

We thank Thomas Buchert, for permitting the use of his software, and Rebecca Danos for permission to use Figure 1 which is taken from [19]. We also wish to thank an anonymous referee for many suggestions on how to improve this work. This research has been supported in

FIG. 7: Minkowski functionals of a combined map (wakes+noise) with $G\mu = 6.7 \times 10^{-8}$ along with the corresponding functionals for a pure noise map, averaged over 100 simulations each using a lattice of 128^3 pixels.



part by an NSERC Discovery Grant, by funds from the

CRC, and by a Killam Research Fellowship.

-
- [1] R. Jeannerot, “A Supersymmetric SO(10) Model with Inflation and Cosmic Strings,” *Phys. Rev. D* **53**, 5426 (1996) [arXiv:hep-ph/9509365];
R. Jeannerot, J. Rocher and M. Sakellariadou, “How generic is cosmic string formation in SUSY GUTs,” *Phys. Rev. D* **68**, 103514 (2003) [arXiv:hep-ph/0308134].
- [2] S. Sarangi and S. H. H. Tye, “Cosmic string production towards the end of brane inflation,” *Phys. Lett. B* **536**, 185 (2002) [arXiv:hep-th/0204074];
E. J. Copeland, R. C. Myers and J. Polchinski, “Cosmic F- and D-strings,” *JHEP* **0406**, 013 (2004) [arXiv:hep-th/0312067].
- [3] R. H. Brandenberger and C. Vafa, “Superstrings in the Early Universe,” *Nucl. Phys. B* **316**, 391 (1989);
A. Nayeri, R. H. Brandenberger and C. Vafa, “Producing a scale-invariant spectrum of perturbations in a Hagedorn phase of string cosmology,” *Phys. Rev. Lett.* **97**, 021302 (2006) [arXiv:hep-th/0511140];
R. H. Brandenberger, A. Nayeri, S. P. Patil and C. Vafa, “String gas cosmology and structure formation,” *Int. J. Mod. Phys. A* **22**, 3621 (2007) [hep-th/0608121];
R. H. Brandenberger, “String Gas Cosmology,” arXiv:0808.0746 [hep-th].
- [4] A. Vilenkin and E.P.S. Shellard, *Cosmic Strings and other Topological Defects* (Cambridge Univ. Press, Cambridge, 1994).
- [5] M. B. Hindmarsh and T. W. B. Kibble, “Cosmic strings,” *Rept. Prog. Phys.* **58**, 477 (1995) [arXiv:hep-ph/9411342].
- [6] R. H. Brandenberger, “Topological defects and structure formation,” *Int. J. Mod. Phys. A* **9**, 2117 (1994) [arXiv:astro-ph/9310041].
- [7] Y. B. Zeldovich, “Cosmological fluctuations produced near a singularity,” *Mon. Not. Roy. Astron. Soc.* **192**, 663 (1980);
A. Vilenkin, “Cosmological Density Fluctuations Produced By Vacuum Strings,” *Phys. Rev. Lett.* **46**, 1169 (1981) [Erratum-ibid. **46**, 1496 (1981)];
N. Turok and R. H. Brandenberger, “Cosmic Strings And The Formation Of Galaxies And Clusters Of Galaxies,” *Phys. Rev. D* **33**, 2175 (1986);
H. Sato, “Galaxy Formation by Cosmic Strings,” *Prog.*

FIG. 8: Minkowski functionals of a combined map (wakes+noise) with $G\mu = 4.3 \times 10^{-8}$ along with the corresponding functionals for a pure noise map, averaged over 100 simulations each using a lattice of 128^3 pixels.

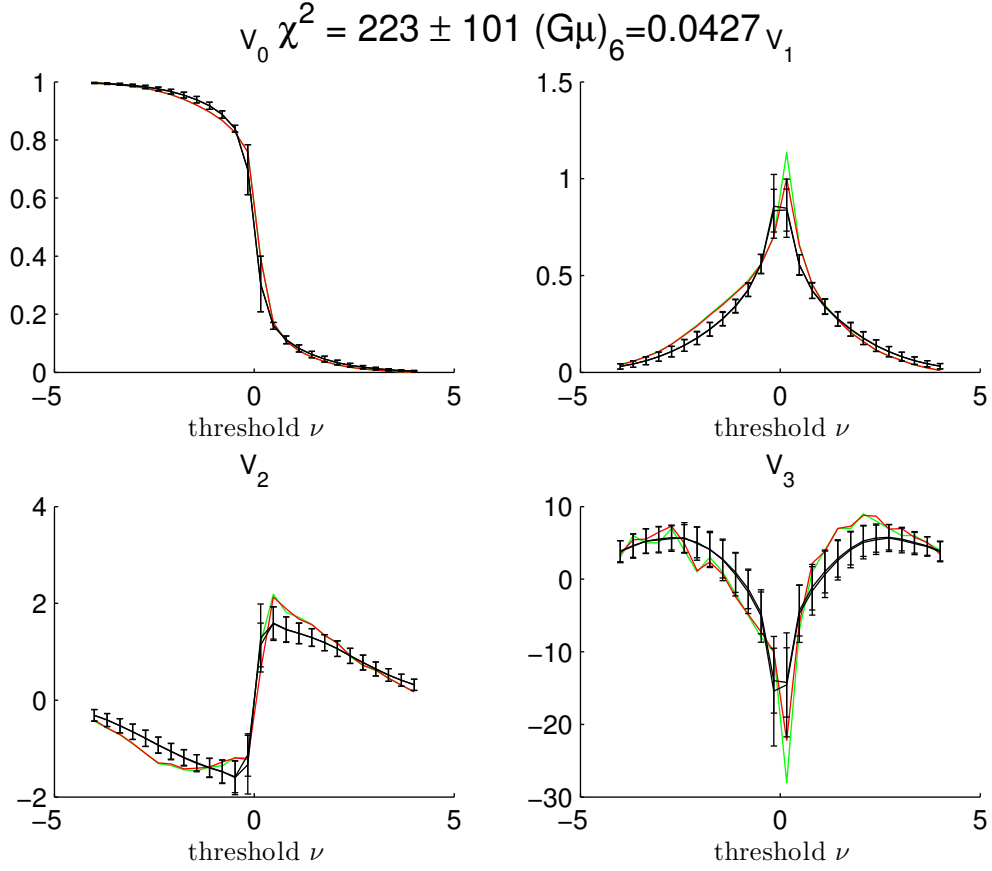
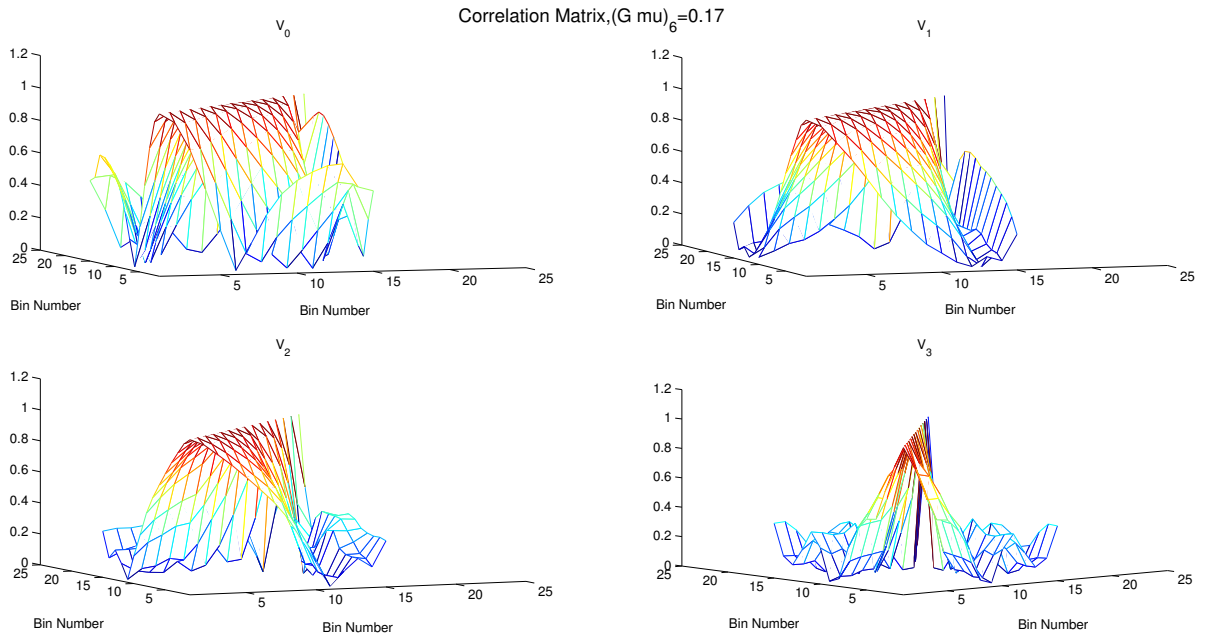


FIG. 9: Correlation of wake signal between bins for each functional, using data from 100 realizations.



- Theor. Phys. **75**, 1342 (1986);
A. Stebbins, “Cosmic Strings and Cold Matter”, Ap. J. (Lett.) **303**, L21 (1986).
- [8] M. Pagano and R. Brandenberger, “The 21cm Signature of a Cosmic String Loop,” JCAP **1205**, 014 (2012) [arXiv:1201.5695 [astro-ph.CO]].
- [9] A. Albrecht and N. Turok, “Evolution Of Cosmic Strings,” Phys. Rev. Lett. **54**, 1868 (1985);
D. P. Bennett and F. R. Bouchet, “Evidence For A Scaling Solution In Cosmic String Evolution,” Phys. Rev. Lett. **60**, 257 (1988);
B. Allen and E. P. S. Shellard, “Cosmic String Evolution: A Numerical Simulation,” Phys. Rev. Lett. **64**, 119 (1990);
C. Ringeval, M. Sakellariadou and F. Bouchet, “Cosmological evolution of cosmic string loops,” JCAP **0702**, 023 (2007) [arXiv:astro-ph/0511646];
A. A. Fraisse, C. Ringeval, D. N. Spergel and F. R. Bouchet, “Small-Angle CMB Temperature Anisotropies Induced by Cosmic Strings,” Phys. Rev. D **78**, 043535 (2008) [arXiv:0708.1162 [astro-ph]];
C. J. A. P. Martins and E. P. S. Shellard, “Fractal properties and small-scale structure of cosmic string networks,” Phys. Rev. D **73**, 043515 (2006) [astro-ph/0511792];
V. Vanchurin, K. D. Olum and A. Vilenkin, “Scaling of cosmic string loops,” Phys. Rev. D **74**, 063527 (2006) [arXiv:gr-qc/0511159];
J. J. Blanco-Pillado, K. D. Olum and B. Shlaer, “Large parallel cosmic string simulations: New results on loop production,” Phys. Rev. D **83**, 083514 (2011) [arXiv:1101.5173 [astro-ph.CO]];
C. Ringeval and F. R. Bouchet, “All sky CMB map from cosmic strings integrated Sachs-Wolfe effect,” arXiv:1204.5041 [astro-ph.CO].
- [10] A. Vilenkin, “Gravitational Field Of Vacuum Domain Walls And Strings,” Phys. Rev. D **23**, 852 (1981);
R. Gregory, “Gravitational Stability of Local Strings,” Phys. Rev. Lett. **59**, 740 (1987).
- [11] J. Silk and A. Vilenkin, “Cosmic Strings And Galaxy Formation,” Phys. Rev. Lett. **53**, 1700 (1984).
- [12] L. Perivolaropoulos, R. H. Brandenberger and A. Stebbins, “Dissipationless Clustering Of Neutrinos In Cosmic String Induced Wakes,” Phys. Rev. D **41**, 1764 (1990);
R. H. Brandenberger, L. Perivolaropoulos and A. Stebbins, “Cosmic Strings, Hot Dark Matter and the Large Scale Structure of the Universe,” Int. J. Mod. Phys. A **5**, 1633 (1990).
- [13] C. Dvorkin, M. Wyman and W. Hu, “Cosmic String constraints from WMAP and the South Pole Telescope,” Phys. Rev. D **84**, 123519 (2011) [arXiv:1109.4947 [astro-ph.CO]].
- [14] L. Pogosian, S. H. H. Tye, I. Wasserman and M. Wyman, “Observational constraints on cosmic string production during brane inflation,” Phys. Rev. D **68**, 023506 (2003) [Erratum-ibid. D **73**, 089904 (2006)] [arXiv:hep-th/0304188];
M. Wyman, L. Pogosian and I. Wasserman, “Bounds on cosmic strings from WMAP and SDSS,” Phys. Rev. D **72**, 023513 (2005) [Erratum-ibid. D **73**, 089905 (2006)] [arXiv:astro-ph/0503364];
A. A. Fraisse, “Limits on Defects Formation and Hybrid Inflationary Models with Three-Year WMAP Observations,” JCAP **0703**, 008 (2007) [arXiv:astro-ph/0603589];
U. Seljak, A. Slosar and P. McDonald, “Cosmological parameters from combining the Lyman-alpha forest with CMB, galaxy clustering and SN constraints,” JCAP **0610**, 014 (2006) [arXiv:astro-ph/0604335];
R. A. Battye, B. Garbrecht and A. Moss, “Constraints on supersymmetric models of hybrid inflation,” JCAP **0609**, 007 (2006) [arXiv:astro-ph/0607339];
R. A. Battye, B. Garbrecht, A. Moss and H. Stoica, “Constraints on Brane Inflation and Cosmic Strings,” JCAP **0801**, 020 (2008) [arXiv:0710.1541 [astro-ph]];
N. Bevis, M. Hindmarsh, M. Kunz and J. Urrestilla, “CMB power spectrum contribution from cosmic strings using field-evolution simulations of the Abelian Higgs model,” Phys. Rev. D **75**, 065015 (2007) [arXiv:astro-ph/0605018];
N. Bevis, M. Hindmarsh, M. Kunz and J. Urrestilla, “Fitting CMB data with cosmic strings and inflation,” Phys. Rev. Lett. **100**, 021301 (2008) [astro-ph/0702223 [ASTRO-PH]];
R. Battye and A. Moss, “Updated constraints on the cosmic string tension,” Phys. Rev. D **82**, 023521 (2010) [arXiv:1005.0479 [astro-ph.CO]].
- [15] A. Guth, “The Inflationary Universe: A Possible Solution To The Horizon And Flatness Problems,” Phys. Rev. D **23**, 347 (1981).
- [16] V. Mukhanov and G. Chibisov, “Quantum Fluctuation And Nonsingular Universe. (In Russian),” JETP Lett. **33**, 532 (1981) [Pisma Zh. Eksp. Teor. Fiz. **33**, 549 (1981)].
- [17] M. Rees, “Baryon concentrations in string wakes at $z \geq 200$: implications for galaxy formation and large-scale structure,” Mon. Not. R. astr. Soc. **222**, 27p (1986);
T. Vachaspati, “Cosmic Strings and the Large-Scale Structure of the Universe,” Phys. Rev. Lett. **57**, 1655 (1986);
A. Stebbins, S. Veeraraghavan, R. H. Brandenberger, J. Silk and N. Turok, “Cosmic String Wakes,” Astrophys. J. **322**, 1 (1987);
J. C. Charlton, “Cosmic String Wakes and Large Scale Structure,” Astrophys. J. **325**, 52 (1988);
T. Hara and S. Miyoshi, “Formation of the First Systems in the Wakes of Moving Cosmic Strings,” Prog. Theor. Phys. **77**, 1152 (1987);
T. Hara and S. Miyoshi, “Large Scale Structures and Streaming Velocities Due to Open Cosmic Strings,” Prog. Theor. Phys. **81**, 1187 (1989).
- [18] R. J. Danos, R. H. Brandenberger and G. Holder, “A Signature of Cosmic Strings Wakes in the CMB Polarization,” Phys. Rev. D **82**, 023513 (2010) [arXiv:1003.0905 [astro-ph.CO]].
- [19] R. H. Brandenberger, R. J. Danos, O. F. Hernandez and G. P. Holder, “The 21 cm Signature of Cosmic String Wakes,” JCAP **1012**, 028 (2010) [arXiv:1006.2514 [astro-ph.CO]].
- [20] O. F. Hernandez, Y. Wang, R. Brandenberger and J. Fong, “Angular 21 cm Power Spectrum of a Scaling Distribution of Cosmic String Wakes,” JCAP **1108**, 014 (2011) [arXiv:1104.3337 [astro-ph.CO]].
- [21] H. Hadwiger, *Vorlesungen über Inhalt, Oberfläche und Isoperimetrie* (Springer, Berlin, 1957).
- [22] K. R. Mecke, T. Buchert, H. Wagner, “Robust morphological measures for large scale structure in the universe,” Astron. Astrophys. **288**, 697-704 (1994). [astro-ph/9312028];

- J. Schmalzing and T. Buchert, “Beyond genus statistics: a unifying approach to the morphology of cosmic structure,” *Astrophys. J.* **482**, L1 (1997) [arXiv:astro-ph/9702130];
- J. Schmalzing, T. Buchert, A. L. Melott, V. Sahni, B. S. Sathyaprakash and S. F. Shandarin, “Disentangling the cosmic web I: morphology of isodensity contours,” *Astrophys. J.* **526**, 568 (1999) [arXiv:astro-ph/9904384].
- [23] D. Novikov, H. A. Feldman and S. F. Shandarin, “Minkowski functionals and cluster analysis for CMB maps,” *Int. J. Mod. Phys. D* **8**, 291 (1999) [arXiv:astro-ph/9809238];
- C. Hikage, E. Komatsu and T. Matsubara, “Primordial Non-Gaussianity and Analytical Formula for Minkowski Functionals of the Cosmic Microwave Background and Large-scale Structure,” *Astrophys. J.* **653**, 11 (2006) [arXiv:astro-ph/0607284];
- S. Winitzki and A. Kosowsky, “Minkowski functional description of microwave background Gaussianity,” *New Astron.* **3**, 75 (1998) [arXiv:astro-ph/9710164].
- [24] D. Mitsouras, R. H. Brandenberger and P. Hickson, “Topological Statistics and the LMT Galaxy Redshift Survey,” arXiv:astro-ph/9806360;
- H. Trac, D. Mitsouras, P. Hickson and R. H. Brandenberger, “Topology of the Las Campanas Redshift Survey,” *Mon. Not. Roy. Astron. Soc.* **330**, 531 (2002) [arXiv:astro-ph/0007125].
- [25] A. Kosowsky [the ACT Collaboration], “The Atacama Cosmology Telescope Project: A Progress Report,” *New Astron. Rev.* **50**, 969 (2006) [arXiv:astro-ph/0608549].
- [26] J. E. Ruhl *et al.* [The SPT Collaboration], “The South Pole Telescope,” *Proc. SPIE Int. Soc. Opt. Eng.* **5498**, 11 (2004) [arXiv:astro-ph/0411122];
- J. E. Carlstrom *et al.*, “The 10 Meter South Pole Telescope,” *Publ. Astron. Soc. Pac.* **123**, 568 (2011) [arXiv:0907.4445 [astro-ph.IM]].
- [27] J. Urrestilla, N. Bevis, M. Hindmarsh, and M. Kunz, “Cosmic string parameter constraints and model analysis using small scale Cosmic Microwave Background data,” *JCAP* **1112**, 021 (2011) [arXiv:1108.2730 [astro-ph.CO]].
- [28] S. Amsel, J. Berger and R. H. Brandenberger, “Detecting Cosmic Strings in the CMB with the Canny Algorithm,” *JCAP* **0804**, 015 (2008) [arXiv:0709.0982 [astro-ph]].
- [29] A. Stewart and R. Brandenberger, “Edge Detection, Cosmic Strings and the South Pole Telescope,” *JCAP* **0902**, 009 (2009) [arXiv:0809.0865 [astro-ph]].
- [30] R. J. Danos and R. H. Brandenberger, “Canny Algorithm, Cosmic Strings and the Cosmic Microwave Background,” *Int. J. Mod. Phys. D* **19**, 183 (2010) [arXiv:0811.2004 [astro-ph]].
- [31] N. Kaiser and A. Stebbins, “Microwave Anisotropy Due To Cosmic Strings,” *Nature* **310**, 391 (1984).
- [32] M. S. Movahed, B. Javanmardi and R. K. Sheth, “Peak-peak correlations in the cosmic background radiation from cosmic strings,” arXiv:1212.0964 [astro-ph.CO].
- [33] T. Vachaspati and A. Vilenkin, “Gravitational Radiation from Cosmic Strings,” *Phys. Rev. D* **31**, 3052 (1985);
- R. L. Davis, “Nucleosynthesis Problems for String Models of Galaxy Formation,” *Phys. Lett.* **B 161**, 285 (1985);
- R. H. Brandenberger, A. Albrecht and N. Turok, “Gravitational Radiation From Cosmic Strings And The Microwave Background,” *Nucl. Phys. B* **277**, 605 (1986).
- [34] D. R. Stinebring, M. F. Ryba, J. H. Taylor and R. W. Romani, “The Cosmic Gravitational Wave Background: Limits From Millisecond Pulsar Timing,” *Phys. Rev. Lett.* **65**, 285 (1990);
- F. R. Bouchet and D. P. Bennett, “Does The Millisecond Pulsar Constrain Cosmic Strings?,” *Phys. Rev. D* **41**, 720 (1990);
- R. R. Caldwell and B. Allen, “Cosmological constraints on cosmic string gravitational radiation,” *Phys. Rev. D* **45**, 3447 (1992);
- S. A. Sanidas, R. A. Battye and B. W. Stappers, “Projected constraints on the cosmic (super)string tension with future gravitational wave detection experiments,” arXiv:1211.5042 [astro-ph.CO];
- S. Kuroyanagi, K. Miyamoto, T. Sekiguchi, K. Takahashi and J. Silk, “Forecast constraints on cosmic strings from future CMB, pulsar timing and gravitational wave direct detection experiments,” arXiv:1210.2829 [astro-ph.CO].
- [35] B. Abbott *et al.* [LIGO Scientific Collaboration], Rept. Prog. Phys. **72**, 076901 (2009) [arXiv:0711.3041 [gr-qc]].
- [36] <http://www.skatelescope.org/>
- [37] <http://www.eso.org/sci/facilities/eelt/>
- [38] See <http://www.lofar.org/>.
- [39] B. W. Holwerda, S. -L. Blyth, A. J. Baker and t. L. team, “Looking At the Distant Universe with the MeerKAT Array (LADUMA),” arXiv:1109.5605 [astro-ph.CO].
- [40] L. Perivolaropoulos, “COBE versus cosmic strings: An Analytical model,” *Phys. Lett. B* **298**, 305 (1993) [arXiv:hep-ph/9208247];
- L. Perivolaropoulos, “Statistics of microwave fluctuations induced by topological defects,” *Phys. Rev. D* **48**, 1530 (1993) [arXiv:hep-ph/9212228].
- [41] S. Furlanetto, S. P. Oh and F. Briggs, “Cosmology at Low Frequencies: The 21 cm Transition and the High-Redshift Universe,” *Phys. Rept.* **433**, 181 (2006) [arXiv:astro-ph/0608032].
- [42] O. F. Hernandez and R. H. Brandenberger, “The 21 cm Signature of Shock Heated and Diffuse Cosmic String Wakes,” *JCAP*, in press (2012), [arXiv:1203.2307 [astro-ph.CO]].
- [43] A. Sornborger, R. H. Brandenberger, B. Fryxell and K. Olson, “The structure of cosmic string wakes,” *Astrophys. J.* **482**, 22 (1997) [arXiv:astro-ph/9608020].
- [44] Paul R. Shapiro and Kyungjin Ahn and Marcelo A. Alvarez and Ilian T. Iliev and Hugo Martel and Dongsu Ryu, “The 21 cm Background from the Cosmic Dark Ages: Minihalos and the Intergalactic Medium before Reionization” *The Astrophysical Journal*, **646**, 2, <http://stacks.iop.org/0004-637X/646/i=2/a=681>, 2006
- [45] I. T. Iliev, K. Ahn, J. Koda, P. R. Shapiro and U. -L. Pen, “Cosmic Structure Formation at High Redshift,” arXiv:1005.2502 [astro-ph.CO].
- [46] W. H. Press and P. Schechter, “Formation of galaxies and clusters of galaxies by selfsimilar gravitational condensation,” *Astrophys. J.* **187**, 425 (1974).
- [47] I. T. Iliev, P. R. Shapiro, A. Ferrara and H. Martel, “On the direct detectability of the cosmic dark ages: 21-cm emission from minihalos,” *Astrophys. J.* **572**, 123 (2002) [astro-ph/0202410].
- [48] P. J. E. Peebles, *The Large-Scale Structure of the Universe* (Princeton Univ. Press, Princeton, 1980).
- [49] H. Minkowski, *Mathematische Annalen* **57**, 447 (1903).
- [50] J. Schmalzing and K. M. Gorski, “Minkowski functionals used in the morphological analysis of cosmic microwave background anisotropy maps,” arXiv:astro-ph/9710185.
- [51] J. Schmalzing, M. Kerscher and T. Buchert, “Minkowski

- functionals in cosmology,” arXiv:astro-ph/9508154.
- [52] H. Tomita, in “Formation, Dynamics and Statistics of Patterns” (Vol. 1) , ed. by K. Kawasaki, M. Suzuki and A. Onuki (World Scientific, Singapore, 1990).
- [53] J. Schmalzing and T. Buchert, “Beyond genus statistics: a unifying approach to the morphology of cosmic structure,” *Astrophys. J.* **482**, L1 (1997) [arXiv:astro-ph/9702130].
- [54] T. Buchert, ‘Minkowski3’, 1997 http://www.cosmunix.de/buchert_software.htm .
- [55] There are also non-inflationary cosmological models like string gas cosmology [3] in which a network of cosmic strings may be produced.
- [56] The network of ‘infinite’ strings can be viewed as a random walk of strings with a step length comparable to the Hubble scale.
- [57] See [9] for simulations of the dynamics of cosmic string networks.
- [58] Whether the signal is in emission or absorption depends on the ratio of the gas temperature in the wake and the CMB background temperature.
- [59] The Fourier space amplitude, on the other hand, does depend on μ [20].
- [60] See also [32] for a different very recent suggestion to search for the string-induced line discontinuities.
- [61] The gravitational wave signals from cosmic string cusps might be larger, but their amplitude is very uncertain.
- [62] Wakes formed at earlier times have smaller angular extent and thickness. The thickness cannot grow until t_{eq} . Hence, such wakes will be less visible than the ones we study.
- [63] This is true if the kinetic temperature which the hydrogen atoms collapsing onto the wakes acquire is larger than $2.5T_g$, where T_g is the temperature of the gas outside of a wake [19]. This will be true for sufficiently large values of $G\mu$. For smaller values, the wake is diffuse [42]. The density contrast inside the wake will be smaller, but the thickness will be larger. These effects will compensate eachother in a Minkowski functional analysis of the wake distribution provided that the smoothing length in the Minkowski code is sufficiently large.